Degradation Effects Related to the Hole Transport Layer in Organic Solar Cells

ARTICLE *in* ADVANCED FUNCTIONAL MATERIALS · JULY 2011

Impact Factor: 11.81 · DOI: 10.1002/adfm.201100429

Degradation Effects Related to the Hole Transport Layer in Organic Solar Cells

*Bernhard Ecker, Jairo Cesar Nolasco, Josep Pallarés, Lluis Francesc Marsal, Jörg Posdorfer, Jürgen Parisi, and Elizabeth von Hauff**

The influence of the hole transport layer on device stability in polymer:fullerene bulk-heterojunction solar cells is reported. Three different hole transport layers varying in composition, dispersion solvent, electrical conductivity, and work function were used in these studies. Two water-based hole transport layers, poly(3,4-ethylenedioxythiophene):poly(styrene sulfonate) and polyaniline:poly(styrene sulfonate), and one isopropyl alcohol-based polyaniline:poly(styrene sulfonate) transport layer were investigated. Solar cells with the different hole transport layers were fabricated and degraded under illumination. Current–voltage, capacitance–voltage, and capacitance–frequency data were collected at light intensities of 16, 30, 48, 80, and 100 mW cm^{-2} over a period of 7 h. Device performance and stability were compared between nonencapsulated and encapsulated samples to gain understanding about degradation effects related to oxygen and water as well as degradation mechanisms related to the intrinsic instability of the solar cell materials and interfaces. It is demonstrated that the properties of the hole transport layer can have a significant impact on the stability of organic solar cells.

1. Introduction

Recently reported certified efficiencies of organic solar cells as high as 8% reflect the rapid development in this area over the past few years.[1] This technology is attractive for photovoltaic applications due to the potential for large area roll-to-roll processing on flexible substrates at low temperatures combined with low cost materials.[2] To bring organic solar cells with full success onto the market, in addition to higher efficiencies and cost-effective processing, longer device lifetimes are necessary.[3] Recent research has been focusing on this subject and two major points regarding the stability and longevity of organic solar cells are addressed in the literature. Firstly, strategies to provide extrinsic stability through the use of proper encapsulation to prevent degradation due to ambient oxygen and water are being investigated, and secondly, research is being conducted to improve the understanding of the intrinsic stability of the different thin film materials and interfaces present in the solar cell in order to isolate the origins of degradation.

To reduce the effects of external factors on the solar cell performance, foils with a low permeation rate for oxygen and water have been applied for encapsulation. An encapsulation which maintains device flexibility is important from the perspective of industrial engineering.[4] A detailed stability study by Reese et al. recently showed that polymer:fullerene films kept at ambient conditions under 1 sun illumination showed a decrease in photoconductivity which was related to the formation of traps in oxidized [6,6]-phenyl-C61-butyric acid methyl ester (PCBM), whereas films kept under inert conditions were stable for a period of 1000 h.[5]

The unique degradation mechanisms affecting the active layer, the interfaces, the transport layers, and the contacts are not yet well understood. A variety of different approaches and techniques is reported in the literature to investigate the intrinsic mechanisms leading to device degradation.[5–9] A study on polymer:fullerene bulk-heterojunction devices demonstrated that the choice of metal for the cathode material has a strong influence on the stability of the devices,[6] and it was shown in a recent study that the incorporation of a C_{60}/LiF interlayer between the active layer and cathode can lead to more stable devices.[10] Another approach recently shown by Chen and Chien uses the spontaneous formation of a poly(ethylene) glycol monolayer on top of the active layer during film formation after blending poly(ethylene) glycol to a P3HT:PCBM solution.[11] This resulted both in higher performance and stability compared to metallic cathodes. Investigations on the anode by Jong et al. showed that the widely used poly(3,4-ethylenedioxythiophene):poly(styrene sulfonate) (PEDOT:PSS), with a pH value between 1 and 2, etches indium out of the indium tin oxide (ITO) anode. This leads to the incorporation of indium in the active layer

B. Ecker, Prof. J. Parisi, Dr. E. von Hauff
Institute of Physics
Energy and Semiconductor Research Laboratory
Carl von Ossietzky University
26111 Oldenburg, Germany
E-mail: elizabeth.v.hauff@uni-oldenburg.de
J. C. Nolasco, Prof. J. Pallarés, Prof. L. F. Marsal
Departament d'Enginyeria Electrònica Elèctrica i Automàtica
Universitat Rovira i Virgili
Avda. Països Catalans 26, 43007 Tarragona, Spain
Dr. J. Posdorfer
Enthone Nano Science Center
Ferdinand-Harten-Str. 7, 22949 Ammersbek, Germany

DOI: 10.1002/adfm.201100429

which can be responsible for decreased life time.[12] Although a variety of oxides, like WO_3,[13] MoO_3, or V_2O_5,[14] or organic materials, like sulfonated poly(diphenylamine), polyaniline (PANI) or (PANI:PSS) were used as hole transport layers in either organic light emitting diodes (OLEDs) or organic solar cells (OSCs), these investigations were mostly conducted in terms of improving device efficiency through different transport layers rather than studying the effect on the stability of the device.[15–18] Studies on the influence of the hole transport layer and the respective interface to the active layer on the stability and lifetime of organic solar cells are still rare. Kawano et al. investigated the influence of air and humidity on ITO/PEDOT:PSS/(poly[2-methoxy-5-(3,7-dimethyloctyloxy)]-1,4-phenylenevinylene) (MDMO-PPV):PCBM/Al solar cells, showing that the hygroscopic nature of PEDOT:PSS can be a significant degradation mechanism in organic solar cells.[19]

Inverted solar cells recently have been shown to have remarkably higher stability compared to organic solar cells in the standard structure, mostly due to the high work function metal anode, which is less sensitive to degradation than low work function metals used as cathodes in noninverted solar cells.[20–22] In inverted solar cells, Norrman et al. identified the PEDOT:PSS layer as one of the main degradation sites via time-of-flight secondary ion mass spectrometry together with isotopic labeling of oxygen and water.[23]

In this study, we investigate the effect of the hole transport layer (HTL) on the stability of polymer:fullerene bulk heterojunction solar cells. We prepared solar cells in the structure depicted in **Figure 1**. A blend of poly-3-hexylthiophene (P3HT):PCBM was used as the active layer. Three different HTLs were investigated, two water-based formulations, (PEDOT:PSS (H_2O)) and (PANI:PSS (H_2O)), and one isopropyl alcohol-based (PANI:PSS (IPA)). The HTLs additionally differed from each other in composition, conductivity, and work function. The characteristics of the HTLs are summarized in **Table 1**. By varying only the HTL between the devices, we were able to isolate the degradation effects related specifically to the HTL interface in the device. We compare the characteristics of nonencapsulated and encapsulated cells to gain insight into the difference between internal and external degradation mechanisms at the HTL interface. We demonstrate that using an appropriate HTL can significantly improve the stability of organic solar cells.

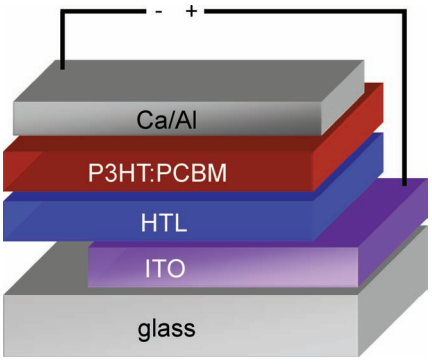

Figure 1. Device layout of the solar cells investigated in this study.

2. Results and Discussion

To investigate the solar cells, current–voltage (*IV*), capacitance–voltage (*CV*) and capacitance–frequency (*Cf*) characteristics were measured under different illumination intensities. Fresh solar cells were measured initially under 1 sun, and subsequent measurements were performed under increasing light intensities, at 16, 30, 48, 80, and 100 mW cm^{-2}. The solar cells were under illumination for a total of 7 h. In **Figure 2**, the initial and final *IV* characteristics of the solar cells at 100 mW cm^{-2} for the nonencapsulated cells (a) and the encapsulated cells (b) are shown. The corresponding solar cell parameters are summarized in **Table 2**.

The cells prepared with PEDOT:PSS (H_2O) initially demonstrated the best performance. This is attributed to the difference in transmittance of the HTLs shown in **Figure 3**. The PEDOT:PSS layer has a higher transmittance compared to the PANI:PSS layer-based solar cells, allowing for more light absorption by the active layer and therefore an increase in the photogeneration of charges, leading to a higher short circuit current density (J_{sc}). Although the work functions of the HTLs vary between 4.81 eV (PEDOT:PSS (H_2O)) and 5.49 eV (PANI:PSS (IPA)) the open circuit voltages (V_{oc}) of the fresh cells are comparable. This is attributed to the pinning of the work function of the HTL to the highest occupied molecular orbital (HOMO) of the polymer.[24]

From the comparison between the initial and final measurements, it can be seen that a decrease in the solar cell performance occurs for both encapsulated and nonencapsulated devices. In the case of the nonencapsulated devices, J_{sc} is significantly diminished between the initial and final measurements in all devices. Additionally, there is a decrease in the fill factor of the devices, and in the case of PEDOT:PSS (H_2O) the V_{oc} is considerably lower after degradation. In general, the sample prepared with PEDOT:PSS (H_2O) shows the largest effects of degradation while the PANI:PSS (IPA) resulted in the most stable devices.

The encapsulated devices were then analyzed in order to understand the intrinsic stability associated with the HTL interface. In this case, the degradation effects in all devices are minimal in comparison to the nonencapsulated devices. J_{sc} remains constant between the initial and final measurements for all the HTLs. A decrease in the fill factor and in V_{oc} is apparent, primarily in the PEDOT:PSS (H_2O)-based device, and to a smaller degree in the PANI:PSS (H_2O)-based device. Again, the PANI:PSS (IPA) HTL results in the least variation between the initial and the final measurements, and these results indicate that using IPA-based HTLs can increase the lifetime of organic solar cells, even in the case of encapsulated devices.

Figure 4 presents mean J_{sc} (a) and V_{oc} (b) values versus light intensity data and the standard deviation for all of the nonencapsulated and encapsulated solar cells investigated. The J_{sc} shows a power law dependence on the illumination intensity (P_{light}) $J_{sc} = P_{light}^{\alpha}$, with $\alpha \sim 1$.[25,26] The V_{oc} varies linearly with the logarithm of the illumination intensity,[25,27] except for the nonencapsulated PEDOT:PSS (H_2O) containing device, where the decrease in V_{oc} due to degradation is apparent.

To obtain deeper insight into the processes involved in the degradation associated with the HTL, we used impedance spectroscopy to investigate the light intensity dependent *Cf* and *CV*

Table 1. Properties of the hole transport layers used in this study.

HTL	Solvent	pH value	Transmittance [%][a)]	Solid content [wt%]	Work function [eV][b)]	Conductivity [S cm^{-1}][c)]
PEDOT:PSS (H_2O)	water	1.5	94	1.5	4.81	3.9 E-4
PANI:PSS (H_2O)	water	1.6	76	3.0	5.08	3.0 E-2
PANI:PSS (IPA)	2-propanol	-	86	2.3	5.49	1.6 E-3

[a)]layer thickness: 100 nm; measured from 400 nm to 900 nm; [b)]measured by Kelvin probe in air at 0% relative humidity and room temperature; [c)]measured in vacuum at room temperature.

characteristics of the solar cells. In inorganic crystalline materials impedance, spectroscopy can be used to probe defect states in the band gap. Trapped charges contribute to the total capacitance of the device, which demonstrate characteristic temperature and frequency dependent relaxation. In the case of disordered organic semiconductors, impedance spectroscopy can be applied to probe the energetic disorder of transport sites in the material. It has been demonstrated in literature that hopping transport in disordered organic semiconductors is mathematically equivalent to band transport with multiple trapping and release processes.[28] An energy range exists at which the hopping rate is maximized. This transport energy (E_T) equates to the mobility edge separating the localized and delocalized states.[29]

Table 2. Open circuit voltage (V_{oc}) and short circuit current density (J_{sc}) of the solar cells presented in Figure 1.

HTL	V_{oc} [mV][a)]	V_{oc} [mV][b)]	J_{sc} [mAcm^{-2}][a)]	J_{sc} [mA cm^{-2}][b)]
PEDOT:PSS (H_2O)[c)]	642.50	606.86	–8.70	–8.69
PANI:PSS (H_2O)[c)]	606.32	581.42	–6.73	–6.57
PANI:PSS (IPA)[c)]	612.64	604.60	–7.69	–7.71
PEDOT:PSS (H_2O)[d)]	614.44	522.07	–8.35	–6.30
PANI:PSS (H_2O)[d)]	617.50	596.90	–6.99	–5.58
PANI:PSS (IPA)[d)]	623.52	607.23	–7.00	–5.94

[a)]initial state; [b)]final state; [c)]encapsulated; [d)]nonencapsulated.

In **Figure 5**a, the *CV* characteristics of the PEDOT:PSS (H_2O)-based device conducted in the dark at frequencies of 5 kHz, 10 kHz, and 50 kHz are shown in the Mott–Schottky representation. The same trend was observed for the other devices (not shown here).

Two regimes with different slopes can be observed from the characteristics, one (I) at around 0 V to +0.5 V and the second (II) at –2 V to 0 V. These regimes are related to the profile of the space charge in the device in inorganic junctions[30] and have been attributed to the contributions from the donor phase (I) and the

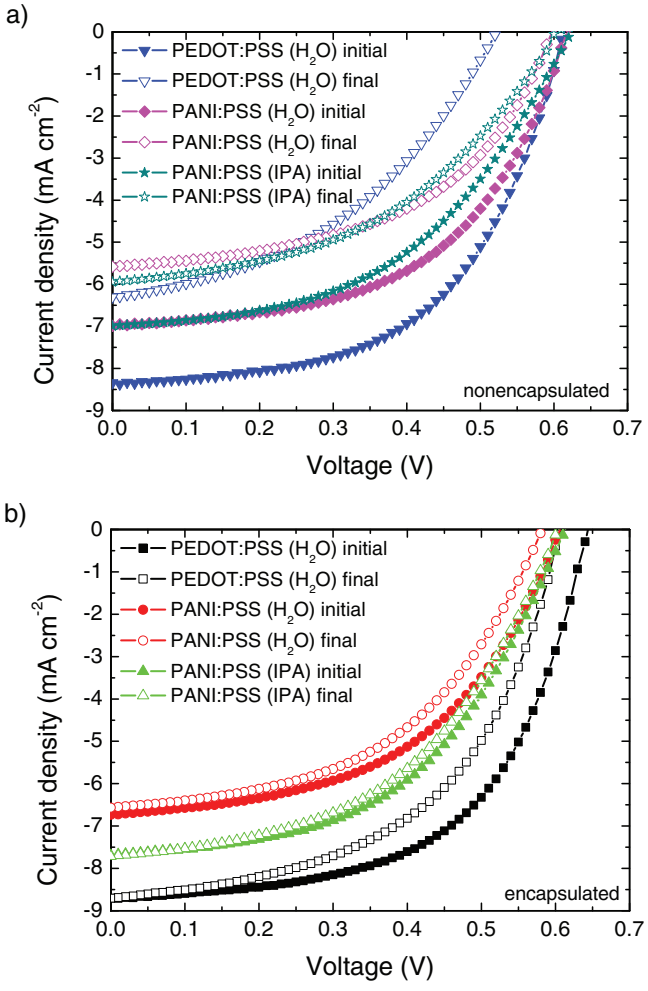

Figure 2. Current density–voltage characteristics of a) nonencapsulated and b) encapsulated solar cells with different hole transport layers at initial and final conditions.

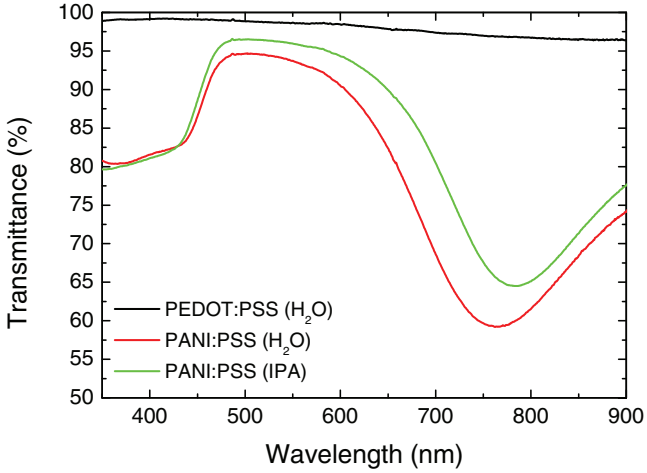

Figure 3. Transmittance spectra of the HTLs investigated using the same preparation conditions as used for the solar cells. Film thicknesses were 35 nm for PEDOT:PSS (H_2O), 63 nm for PANI:PSS (H_2O) and 121 nm for PANI:PSS (IPA).

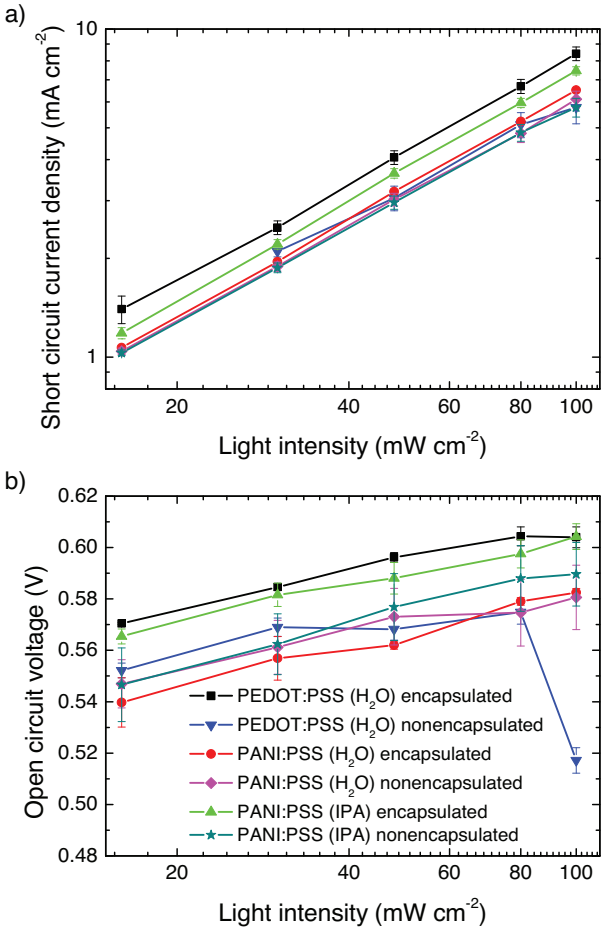

Figure 4. a) Short circuit current density (J_{sc}) and b) open circuit voltage (V_{oc}) of the solar cells presented in Figure 1 plotted versus light intensity. A clear deviation of V_{oc} of the nonencapsulated device from the logarithmic behavior with increasing light intensity can be observed.

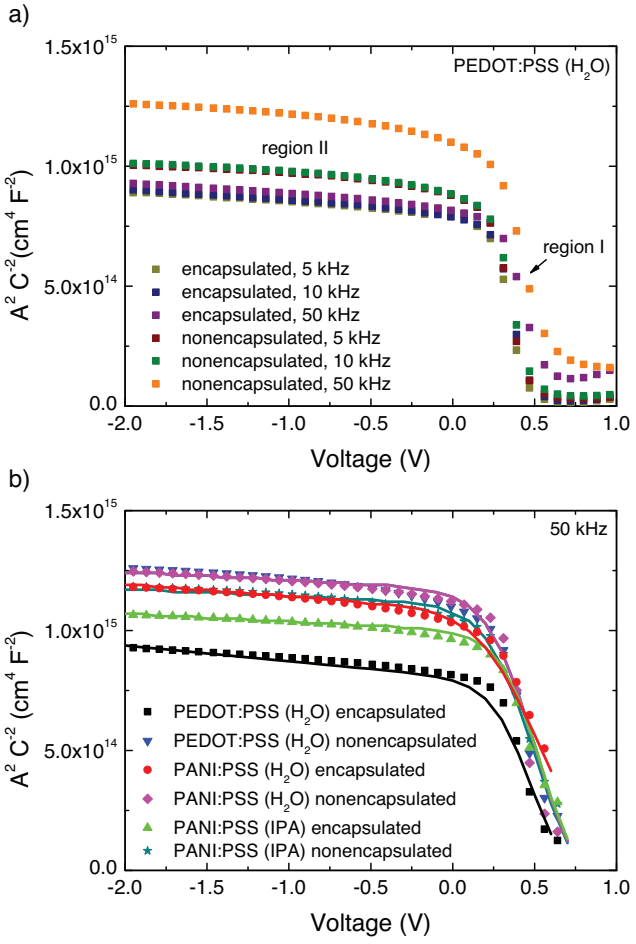

Figure 5. Mott–Schottky representation of experimental capacitance–voltage data (symbols) measured in the dark of a) encapsulated and nonencapsulated devices containing PEDOT:PSS (H_2O) as hole transport layer and b) simulations (lines) compared to experimental data (symbols) of the different hole transport layers at an applied frequency of 50 kHz.

acceptor phase (II) in organic solar cells.[31] Probing the capacitance vs. voltage over different frequencies demonstrates that the slopes in both regions I and II remain constant but a shift in the characteristics with increasing frequencies to higher forward voltages can be observed. This implies that the built-in voltages, which are given by the extrapolated interception of the respective region with the voltage axis, depend on the frequency applied during the measurement, an indication that interface traps are present.[32,33]

The charge carrier concentration from region I (P3HT), under the assumption that $N_{PCBM} >> N_{P3HT}$, can be extracted referring to the classical abrupt junction model.[34] To calculate the charge carrier concentration N_{P3HT} the standard Schottky–Mott analysis was used:[32]

$$\left(\frac{A}{C}\right)^2 = \frac{2\,(V - V_{Bi})}{q\;\varepsilon_0\;\varepsilon_{P3HT}\;N_{P3HT}} \tag{1}$$

where A is the active area of the solar cell, C is the capacitance, V is the applied voltage, V_{Bi} is the built-in voltage, q is the elementary charge, ε_0 is the vacuum permittivity, ε_{P3HT} is the relative dielectric constant of P3HT. Applying Equation 1 to the CV characteristics recorded at 50 kHz for the various illumination intensities we obtain the charge carrier concentration in the P3HT phase vs. light intensity shown in **Figure 6**a.

To calculate the charge carrier concentration in the PCBM phase N_{PCBM} (region II), we assume that the P3HT phase is fully depleted of free charges, and the following relation was applied:[30,31]

$$V_{II} = V_{Bi} + \left(\frac{q}{2\,\varepsilon_0\,\varepsilon_{PCBM}}\right) N_{PCBM}\,t^2 \tag{2}$$

Where V_{II} is the intercept of region II with the voltage axis, ε_{PCBM} is the relative dielectric constant of PCBM and t is the thickness of the P3HT phase. The calculated charge carrier concentration of the PCBM phase vs. light intensity is shown in Figure 6b.

The extracted free charge carrier concentrations of P3HT and PCBM were used in AFORSHET V2.2 to simulate CV data. The simulated data (lines) is presented together with the experimental data for the CV characteristics (symbols) at 50 kHz in Figure 5b and demonstrate good agreement. An error in the sample thickness of 15 nm and in the charge carrier concentration of 4×10^{15} cm^{-3} was found.

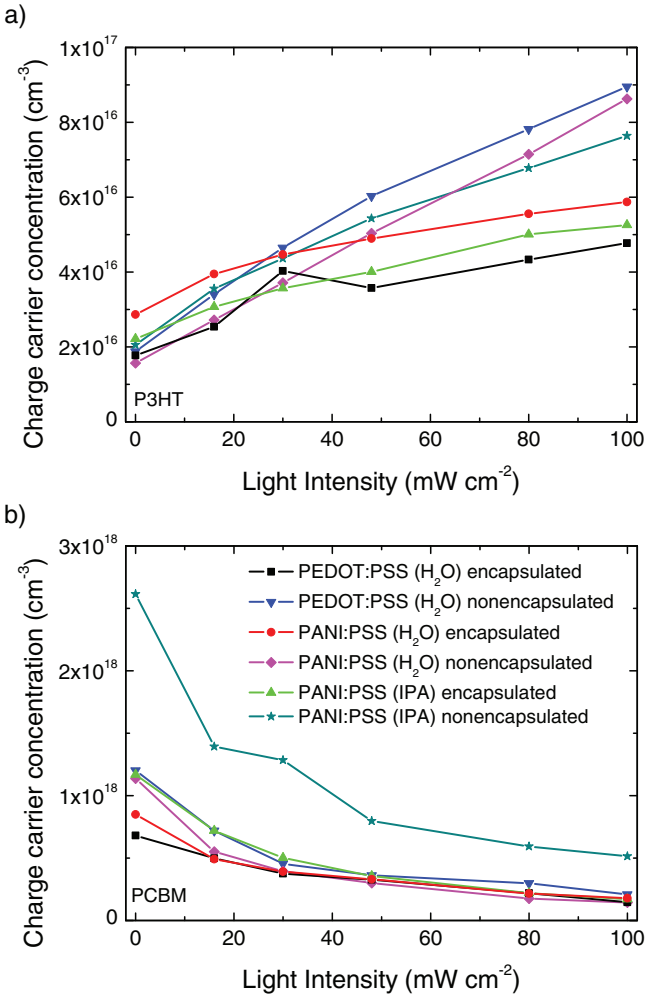

Figure 6. Charge carrier concentration in a) P3HT and b) PCBM plotted versus illumination intensity. Values extracted from *CV* measurements taken at 50 kHz.

In the case of P3HT, it can be seen that the charge carrier concentration increases with light intensity for all the devices, as expected for the photogeneration of charges in the bulk. There is an increase in the slope of the characteristics in the nonencapsulated devices compared to the encapsulated devices. This is attributed to oxygen doping, which introduces trap states for electrons into the bulk.[8] This can result in an increase in the hole density in the polymer. In the case of PCBM, there is a slight decrease observed in the charge carrier concentration with increasing illumination intensity and degradation time for all devices. This could be due to increased oxidation of the polymer or fullerene with degradation time.[5,35] A decrease of the charge carrier concentration in the acceptor phase has also been observed in degraded solar cells with a copper phthalocyanine(CuPc):N,N′-bis(2-phenylethyl)-perylene-3,4,9,10-tetracarbonicacid-diimide (BPE-PTCDI) heterojunction.[34]

Using *Cf* measurements, we calculated the density of states (DOS) as proposed by Walter et al. for noncrystalline, inorganic materials, which was recently applied by Reis et al. for polymer diodes and by Boix et al. for polymer:fullerene solar cells:[36–38]

$$\mathrm{DOS}(E) = -\frac{V_{\mathrm{Bi}}\omega}{t\,q\,k_{\mathrm{B}}\,T}\frac{\partial C}{\partial \omega} \tag{3}$$

Where, E is the energy, V_{Bi} is the built-in voltage, ω is the angular frequency, k_{B} is the Boltzmann factor and T is the temperature. The assumption in Equation 3 is that variations in the capacitance of the device with frequency directly correspond to trapping and release of charge by trap sites in the band gap close to the Fermi energy (E_{F}). In the case of disordered organic materials, we understand this to equate to probing transport sites close to E_{F} located energetically below E_{T}. In order to convert the angular frequency dependent DOS into the energy dependent DOS, we used:[36]

$$E = k_{\mathrm{B}}\,T\,In\frac{2\beta\,N}{\omega} \tag{4}$$

where β is the capture cross section and N is the effective density of states. In this study we assumed a value for β, which usually can be extracted from temperature dependent measurements. It should be noted that changes in β only result in a shift of the DOS on the energy scale, and not a change in the shape of the distribution. In the following, we examine the influence of the different HTLs on the shape of the DOS.

Figure 7a presents the calculated DOS at open circuit conditions at illumination intensities of 16 mW cm^{-2} (at the start of the degradation process) and 100 mW cm^{-2} (after degradation), respectively. Two Gaussian distributions at different energetic positions are present. We attribute the Gaussian at lower energies to the DOS in the active layer, as the distribution is common to all the devices. From this analysis, it is not possible to distinguish between contributions from the electron and hole sites to the DOS.[36] The higher noise ratio for the distribution at higher energies is an indication that this distribution accounts for the HTL interface as it also varies between the samples containing different HTLs and is accompanied by flicker noise.[39] The hole transport layers for both encapsulated and nonencapsulated devices show a similar behavior at 16 mW cm^{-2}, as the devices are still fresh.

At 100 mW cm^{-2} (Figure 7b), the distribution related to the bulk is shifted towards slightly lower energies and a broadening of the distribution is observed. This effect is more apparent in the nonencapsulated devices but also visible in the encapsulated devices. This effect may be due to the increase in charge carrier concentration at higher light intensities, leading to the filling of higher energy states. It may, however, also be a result of degradation, specifically of traps due to oxygen in the case of the nonencapsulated devices in addition to internal instabilities in the bulk, such as changes to the morphology, for both nonencapsulated and encapsulated devices.

The distribution related to the HTL interface also demonstrates a broadening in form and the DOS is shifted away from the bulk related distribution to higher energies compared to the initial data at 16 mW cm^{-2}. Interestingly, in the case of the water-based HTLs, an additional shoulder becomes visible, which is prominent for the PEDOT:PSS (H$_2$O) and also observed for the PANI:PSS (H$_2$O). Additional Gaussian fits in this energy range reveal distributions, which are attributed to the formation of additional trap states at the interface between the HTL and bulk. This is a clear indication that the choice of

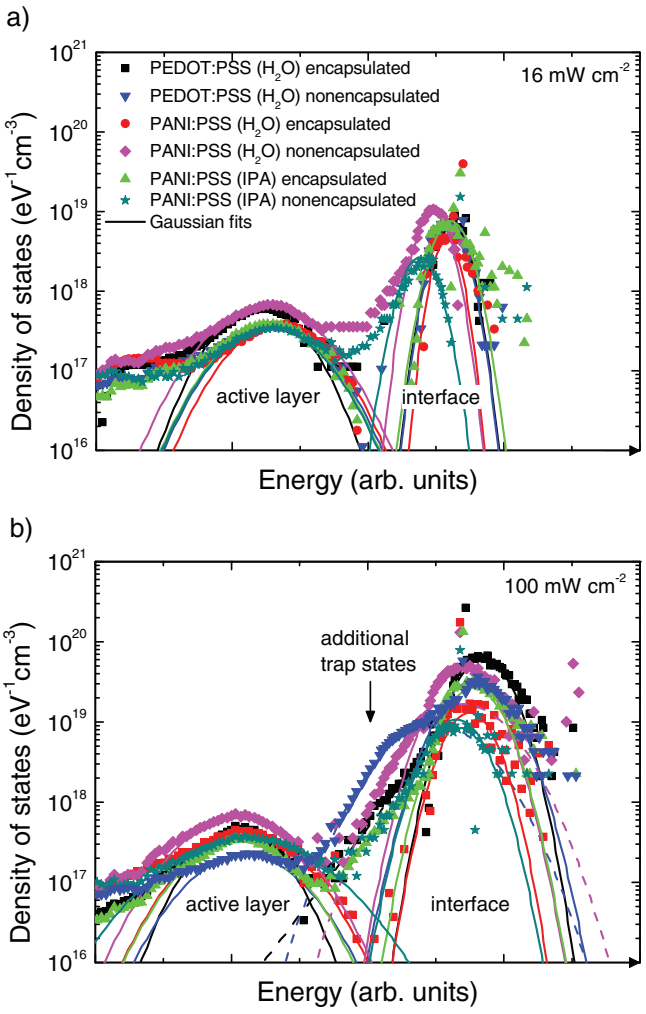

Figure 7. Density of states (DOS) plotted vs. energy for devices illuminated with 16 mW cm^{-2} and 100 mW cm^{-2}, respectively, under open circuit conditions. Lines show Gaussian fits to states attributed to the bulk and interface. Dashed lines are Gaussian fits to states originating to interfacial trap states.

solvent of the HTL has a major impact on device stability, which is improved with IPA-based solvents over water-based solvents.

Based on these results, it is apparent that the properties of the HTL can have a significant impact on the stability of organic solar cells. The effects of the HTL properties (composition, solvent, and work function) on the performance of the solar cell were investigated. It was seen that PEDOT:PSS (H_2O) resulted in the best initial performance for the solar cells investigated here. This was attributed to the higher transmittance of the PEDOT:PSS (H_2O). The work function of the HTL were not observed to influence the initial solar cell performance. The solvent of the HTL was observed to have an effect on the device stability. The IPA-based HTL resulted in the most stable device, while the water-based HTLs led to a more rapid deterioration in the solar cell performance.

In literature it was observed that the acidic pH of water-based HTLs can lead to a degradation of the anode interface and an etching of the indium from the ITO electrode, resulting in a diffusion of indium throughout the device.[12,19] Chang and Chen demonstrated that the dissolving of indium in PEDOT:PSS (H_2O) also leads to a decrease of its work function.[40] This would result in degradation even in encapsulated solar cells, primarily in the fill factor and V_{oc}, as observed here. In the case of the nonencapsulated solar cells, ambient water entering the solar cell can be absorbed by the hygroscopic water-based HTLs leading to further degradation of the HTL interface. Future studies are planned to clarify the detailed properties of the HTL responsible for improved device stability.

3. Conclusions

We demonstrate that the properties of the HTL can have a significant influence on the stability of organic solar cells. We compared the effect of using PEDOT:PSS (H_2O), PANI:PSS (H_2O) and PANI:PSS (IPA) on device stability. The transmittance of the HTL influences the J_{sc}, resulting in the initially highest J_{sc} for the PEDOT:PSS (H_2O) device. The stability of the solar cell was observed to be lower in the devices prepared with water-based HTLs compared to devices prepared using the IPA-based HTL, particularly in the case of nonencapsulated devices. In encapsulated devices, an increase in the intrinsic stability can be observed for the solar cells prepared with the IPA-based HTL. Charge carrier concentrations extracted from *CV* measurements revealed a minimal impact of the ambient conditions on the degradation of the bulk-heterojunction. Degradation effects at the HTL interface, however, were found to be significant, and lead to a shift of the built-in voltage with increasing probing frequency. Finally, the DOS calculated from *Cf* measurements shows additional trap states for nonencapsulated water-based HTLs at the HTL interface.

4. Experimental Section

Sample Preparation: A 1 wt% 2:1 P3HT:PCBM blend was prepared under inert atmosphere in chlorobenzene and kept stirring for several days prior solar cell preparation. P3HT and PCBM were obtained from Rieke Metals, Inc. and Solenne BV, respectively. ITO covered glass substrates were structured by etching in hydrochloric acid and mechanically cleaned with detergent and deionized water. Subsequent cleaning was done for 10 min in acetone and isopropyl alcohol using an ultrasonic bath followed by an oxygen plasma treatment for 15 min. Hole transport layers were spin coated onto the cleaned substrates in ambient conditions at 3500 rpm for 30 s. The PEDOT:PSS-based HTL investigated here was Clevios P VP AI 4083 from H.C. Starck (applied using a 45 µm pore filter) and HTLs based on PANI:PSS were obtained from Ormecon GmbH, a business of Enthone Inc., and used as received. The water-based dispersion D 1022 W-1 and an isopropyl alcohol-based dispersion, which was derived from D 1034 W by solvent exchange, was used. Due to the same spin coating parameters but higher solid content in PANI:PSS-based HTLs, thicker and therefore not yet optimized films of PANI:PSS were obtained.

After deposition of the HTL, the samples were brought into a nitrogen filled glove box where all subsequent steps were carried out. The HTL covered substrates were dried on a hot plate at 130 °C for 10 min. The P3HT:PCBM solution was spin coated on top of the HTLs resulting in an active layer thickness around 100 nm. The substrates were then transferred into an evaporation chamber. Calcium and aluminum were evaporated on top of the active layer in vacuum below 10^{-6} mbar, with thicknesses of 20 nm and 150 nm, respectively. The overlap of ITO and

the metal cathode defined the solar cell area $A = 0.5$ cm^2. The devices were then annealed on a hot plate at 140 °C for 10 min.

Encapsulation of the devices was also done under inert atmosphere using a 1:1 mixture of an epoxy resin and adequate hardener, which was sandwiched between the organic solar cell device and a cover glass plate.

Characterization: *IV* characteristics of the devices were measured with a Keithley 4200 Semiconductor Characterization System in four point configuration, impedance spectroscopy was carried out using a Solartron 1260 analyzer, set to an AC amplitude of $V_{rms} = 100$ mV. The device temperature was kept in a range of 29.8 °C ± 5 °C using a cooling stage for measurements under illumination with a solar simulator (K. H. Steuernagel Technical Lightning) at an intensity of ~100 mW cm^{-2}. The intensity was measured using a silicon solar cell, calibrated at Fraunhofer ISE. Lower light intensities were obtained by using various shading grids inserted on the output of the sun simulator.

Acknowledgements

The Oldenburg Group acknowledges funding from the EWE-Nachwuchsgruppe "Dünnschichtphotovoltaik" by the EWE AG Oldenburg, the Federal Ministry of Education and Research (BMBF) (EOS) and the Universitätsgesellschaft Oldenburg e.V. The URV Group acknowledges funding from Spanish Ministry of Science and Innovation (MICINN) under grant number TEC2009-09551, CONSOLIDER HOPE project CSD2007-00007 and scholarship TME2009-00401. The authors thank the Helmholtz Centre for Materials and Energy, Berlin, for free public release of AFORSHET.

Received: February 24, 2011
Published online: May 24, 2011

[1] http://www.pv-tech.org/news/_c/opv_dssc/, last accessed Nov. **2010**.
[2] C. J. Brabec, S. Gowrisanker, J. J. M. Halls, D. Laird, S. Jia, S. P. Williams, *Adv. Mater.* **2010**, *22*, 3839.
[3] M. Jørgensen, K. Norrman, F. C. Krebs, *Sol. Energy Mater. Sol. Cells* **2008**, *92*, 686.
[4] J. Hauch, P. Schilinsky, S. Choulis, R. Childers, M. Biele, C. J. Brabec, *Sol. Energy Mater. Sol. Cells* **2008**, *92*, 727.
[5] M. O. Reese, A. M. Nardes, B. L. Rupert, R. E. Larsen, D. C. Olson, M. T. Lloyd, S. E. Shaheen, D. S. Ginley, G. Rumbles, N. Kopidakis, *Adv. Funct. Mater.* **2010**, *20*, 3476.
[6] M. O. Reese, A. J. Morfa, M. S. White, N. Kopidakis, S. E. Shaheen, G. Rumbles, D. S. Ginley, *Sol. Energy Mater. Sol. Cells* **2008**, *92*, 746.
[7] J. Schafferhans, A. Baumann, A. Wagenpfahl, C. Deibel, V. Dyakonov, *Org. Electron.* **2010**, *11*, 1693.
[8] A. Seemann, H.-J. Egelhaaf, C. J. Brabec, J. Hauch, *Org. Electron.* **2009**, *10*, 1424.
[9] K. Kawano, C. Adachi, *Adv. Funct. Mater.* **2009**, *19*, 3934.
[10] K. Kawano, C. Adachi, *Appl. Phys. Lett.* **2010**, *96*, 053307.
[11] F.-C. Chen, S.-C. Chien, *J. Mat. Chem.* **2009**, *19*, 6865.
[12] M. P. D. Jong, L. J. V. Ijzendoorn, M. J. A. D. Voigt, *Appl. Phys. Lett.* **2000**, *77*, 2255.
[13] C. Tao, S. Ruan, G. Xie, X. Kong, L. Shen, F. Meng, C. Liu, X. Zhang, W. Dong, W. Chen, *Appl. Phys. Lett.* **2009**, *94*, 043311.
[14] V. Shrotriya, G. Li, Y. Yao, C.-W. Chu, Y. Yang, *Appl. Phys. Lett.* **2006**, *88*, 073508.
[15] C.-Y. Li, T.-C. Wen, T.-H. Lee, T.-F. Guo, J.-C.-A. Huang, Y.-C. Lin, Y.-J. Hsu, *J. Mater. Chem.* **2009**, *19*, 1643.
[16] G. Gustafsson, Y. Cao, G. M. Treacy, F. Klavetter, N. Colaneri, A. J. Heeger, *Nature* **1992**, *357*, 477.
[17] H. Bejbouji, L. Vignau, J. L. Miane, M.-T. Dang, E. M. Oualim, M. Harmouchi, A. Mouhsen, *Sol. Energy Mater. Sol. Cells* **2010**, *94*, 176.
[18] H. Bejbouj, L. Vignau, J. L. Miane, T. Olinga, G. Wantz, A. Mouhsen, E. M. Oualim, M. Harmouchi, *Mater. Sci. Eng. B* **2010**, *166*, 185.
[19] K. Kawano, R. Pacios, D. Poplavskyy, J. Nelson, D. Bradley, J. Durrant, *Sol. Energy Mater. Sol. Cells* **2006**, *90*, 3520.
[20] B. Zimmermann, U. Würfel, M. Niggemann, *Sol. Energ. Mat. Sol. C.* **2009**, *93*, 491.
[21] S. K. Hau, H.-L. Yip, N. S. Baek, J. Zou, K. O'Malley, A. K.-Y. Jen, *Appl. Phys. Lett.* **2008**, *92*, 253301.
[22] M. T. Lloyd, D. C. Olson, P. Lu, E. Fang, D. L. Moore, M. S. White, M. O. Reese, D. S. Ginley, J. W. P. Hsu, *J. Mat. Chem.* **2009**, *19*, 7638.
[23] K. Norrman, M. V. Madsen, S. Gevorgyan, F. C. Krebs, *J. Am. Chem. Soc.* **2010**, *132*, 16883.
[24] S. Braun, W. R. Salaneck, M. Fahlman, *Adv. Mater.* **2009**, *21*, 1450.
[25] I. Riedel, J. Parisi, V. Dyakonov, L. Lutsen, D. Vanderzande, J. C. Hummelen, *Adv. Funct. Mater.* **2004**, *14*, 38.
[26] L. J. Koster, V. D. Mihailetchi, H. Xie, P. W. M. Blom, *Appl. Phys. Lett.* **2005**, *87*, 203502.
[27] L. J. Koster, V. D. Mihailetchi, R. Ramaker, P. W. M. Blom, *Appl. Phys. Lett.* **2005**, *86*, 123509.
[28] S. D. Baranovskii, H. Cordes, F. Hensel, *Phys. Rev. B* **2000**, *62*, 7934.
[29] D. Monroe, *Phys. Rev. Lett.* **1985**, *54*, 146.
[30] K. L. Chopra, S. R. Das, *Thin Film Solar Cells*, Plenum, New York **1983**.
[31] J. C. Nolasco, A. Sánchez-Díaz, R. Cabré, J. Ferré-Borrull, L. F. Marsal, E. Palomares, J. Pallarès, *Appl. Phys. Lett.* **2010**, *97*, 013305.
[32] S. M. Sze, *Physics Of Semiconductor Devices*, Wiley, New York **2007**.
[33] I. Torres, D. M. Taylor, E. Itoh, *Appl. Phys. Lett.* **2004**, *85*, 314.
[34] A. Liu, S. Zhao, S.-B. Rim, J. Wu, M. Könemann, P. Erk, P. Peumans, *Adv. Mater.* **2008**, *20*, 1065.
[35] H. Hintz, H. J. Egelhaaf, H. Peisert, T. Chassé, *Polym. Degrad. Stab.* **2010**, *95*, 818.
[36] T. Walter, R. Herberholz, C. Mueller, H. W. Schock, *J. Appl. Phys.* **1996**, *80*, 4411.
[37] F. T. Reis, L. F. Santos, R. F. Bianchi, H. N. Cunha, *Appl. Phys. A* **2009,** *96*, 909.
[38] P. P. Boix, G. Garcia-Belmonte, U. Muñecas, M. Neophytou, C. Waldauf, R. Pacios, *Appl. Phys. Lett.* **2009**, *95*, 233302.
[39] O. D. Jurchescu, B. H. Hamadani, H. D. Xiong, S. K. Park, S. Subramanian, N. M. Zimmerman, J. E. Anthony, T. N. Jackson, D. J. Gundlach, *Appl. Phys. Lett.* **2008**, *92*, 132103.
[40] C.-H. Chang, S.-A. Chen, *Appl. Phys. Lett.* **2007**, *91*, 103514.